LETTER

doi:10.1038/nature12534

Recent global-warming hiatus tied to equatorial Pacific surface cooling

Yu Kosaka[1] & Shang-Ping Xie[1,2,3]

Despite the continued increase in atmospheric greenhouse gas concentrations, the annual-mean global temperature has not risen in the twenty-first century[1,2], challenging the prevailing view that anthropogenic forcing causes climate warming. Various mechanisms have been proposed for this hiatus in global warming[3–6], but their relative importance has not been quantified, hampering observational estimates of climate sensitivity. Here we show that accounting for recent cooling in the eastern equatorial Pacific reconciles climate simulations and observations. We present a novel method of uncovering mechanisms for global temperature change by prescribing, in addition to radiative forcing, the observed history of sea surface temperature over the central to eastern tropical Pacific in a climate model. Although the surface temperature prescription is limited to only 8.2% of the global surface, our model reproduces the annual-mean global temperature remarkably well with correlation coefficient $r = 0.97$ for 1970–2012 (which includes the current hiatus and a period of accelerated global warming). Moreover, our simulation captures major seasonal and regional characteristics of the hiatus, including the intensified Walker circulation, the winter cooling in northwestern North America and the prolonged drought in the southern USA. Our results show that the current hiatus is part of natural climate variability, tied specifically to a La-Niña-like decadal cooling. Although similar decadal hiatus events may occur in the future, the multi-decadal warming trend is very likely to continue with greenhouse gas increase.

Daily mean carbon dioxide at Mauna Loa of Hawaii exceeded 400 parts per million (p.p.m.) for the first time in May 2013. Whereas greenhouse gas increase has been shown to cause the centennial trend of global temperature rise since the industrial revolution[7], global temperature has remained flat for the past 15 years (Extended Data Fig. 1). Two schools of thought exist regarding the cause of this hiatus in global warming: one suggests a slowdown in radiative forcing due to the stratospheric water vapour[3], the rapid increase of stratospheric and tropospheric aerosols[4,5], and the solar minimum around 2009 (ref. 5); and the other considers the hiatus to be part of natural variability, especially influenced by a La-Niña-like cooling in the tropical Pacific[6].

A quantitative method is necessary to evaluate the relative importance of these mechanisms. Adding to the confusion surrounding the global warming hiatus, record heat waves hit Russia (summer 2010) and the USA (July 2012), and Arctic sea ice reached record lows in 2007 and 2012 (Extended Data Fig. 1). Discovering the causes of these regional climate changes requires a dynamic approach. Here we used an advanced climate model that takes radiative forcing and tropical Pacific sea surface temperature (SST) as inputs. The simulated global-mean temperature is in excellent agreement with observations, showing that the decadal cooling of the tropical Pacific causes the current hiatus. Our dynamic-model-based attribution has a distinct advantage over the empirical approach[2,5] in that it reveals seasonal and regional aspects of the hiatus.

Three sets of experiments were performed, using the Geophysical Fluid Dynamics Laboratory coupled model version 2.1 (ref. 8). The historical (HIST) experiment is forced with observed atmospheric composition changes and the solar cycle. In Pacific Ocean–Global Atmosphere (POGA) experiments, SST anomalies in the equatorial eastern Pacific (8.2% of the Earth's surface) follow the observed evolution (see Methods). In POGA-H, the radiative forcing is identical to HIST, and in the POGA control experiment (POGA-C) it is fixed at the 1990 value. Outside the equatorial eastern Pacific, the atmosphere and ocean are fully coupled and free to evolve.

Figure 1 compares the observed and simulated global near-surface temperature. In HIST, the annual-mean temperature keeps rising in response to the increased radiative forcing, with expanding departures from observations for the recent decade (Fig. 1a). POGA-H reproduces the observed record well (Extended Data Table 1). For a 43-year period after 1970 when equatorial Pacific SST data are more reliable, the correlation with observations is $r = 0.97$ for POGA-H, due largely to the long-term trend ($r = 0.90$ for HIST). Detrended, POGA-H still reproduces the observations at $r = 0.70$, whereas it falls to 0.26 in HIST. POGA-C illustrates the tropical control of the global temperature with constant radiative forcing, with the global-mean temperature closely following tropical Pacific variability (Fig. 1b). The global-mean surface air temperature (SAT) changes by 0.29 °C in response to a 1 °C SAT anomaly over the equatorial eastern Pacific. For the recent decade, the decrease in tropical Pacific SST has lowered the global temperature by about 0.15 °C compared to the 1990s (Fig. 1b), opposing the radiative forcing effect and causing the hiatus. Likewise an El-Niño-like trend in the tropics[9] accelerated the global warming from the 1970s to late 1990s[10] (Extended Data Table 1).

The POGA experimental design has been used to study the global teleconnections of the interannual El Niño/Southern Oscillation (ENSO)[11,12]. Here we present a novel application of POGA and demonstrate its ability to simulate the observed decadal modulations of the global warming trend, including the peculiar hiatus. Our results show that the two-parameter (radiative forcing and tropical Pacific SST) system is remarkably good at reproducing the observed global-mean temperature record, better than the HIST results with radiative forcing alone. In individual HIST realizations, hiatus events feature decadal La-Niña-like cooling in the tropical Pacific[6] (Extended Data Fig. 2), but POGA-H enables a direct year-by-year comparison with the observed time series of global temperature, not just the statistics from unconstrained coupled runs.

We focused on trends over the recent 11 years from 2002 to 2012, to avoid the strong 1997/98 El Niño event and the following three-year La Niña events. Net downward radiation and ocean heat content in POGA-H have continued to increase during the global SAT hiatus[6] (Extended Data Fig. 3). The SAT hiatus is confined to the cold season[13] (seasons refer to those for the Northern Hemisphere hereafter), with a decadal cooling trend for November to April, whereas the global temperature continues to rise during summer (Fig. 1c). POGA-H reproduces this seasonal cycle of the hiatus, albeit with a somewhat reduced amplitude. Although the La-Niña-like cooling trend in the tropical

[1]Scripps Institution of Oceanography, University of California, San Diego, 9500 Gilman Drive MC 206, La Jolla, California 92093-0206, USA. [2]Physical Oceanography Laboratory and Ocean–Atmosphere Interaction and Climate Laboratory, Ocean University of China, 238 Songling Road, Qingdao 266100, China. [3]International Pacific Research Center, SOEST, University of Hawaii at Manoa, 1680 East West Road, Honolulu, Hawaii 96822, USA.

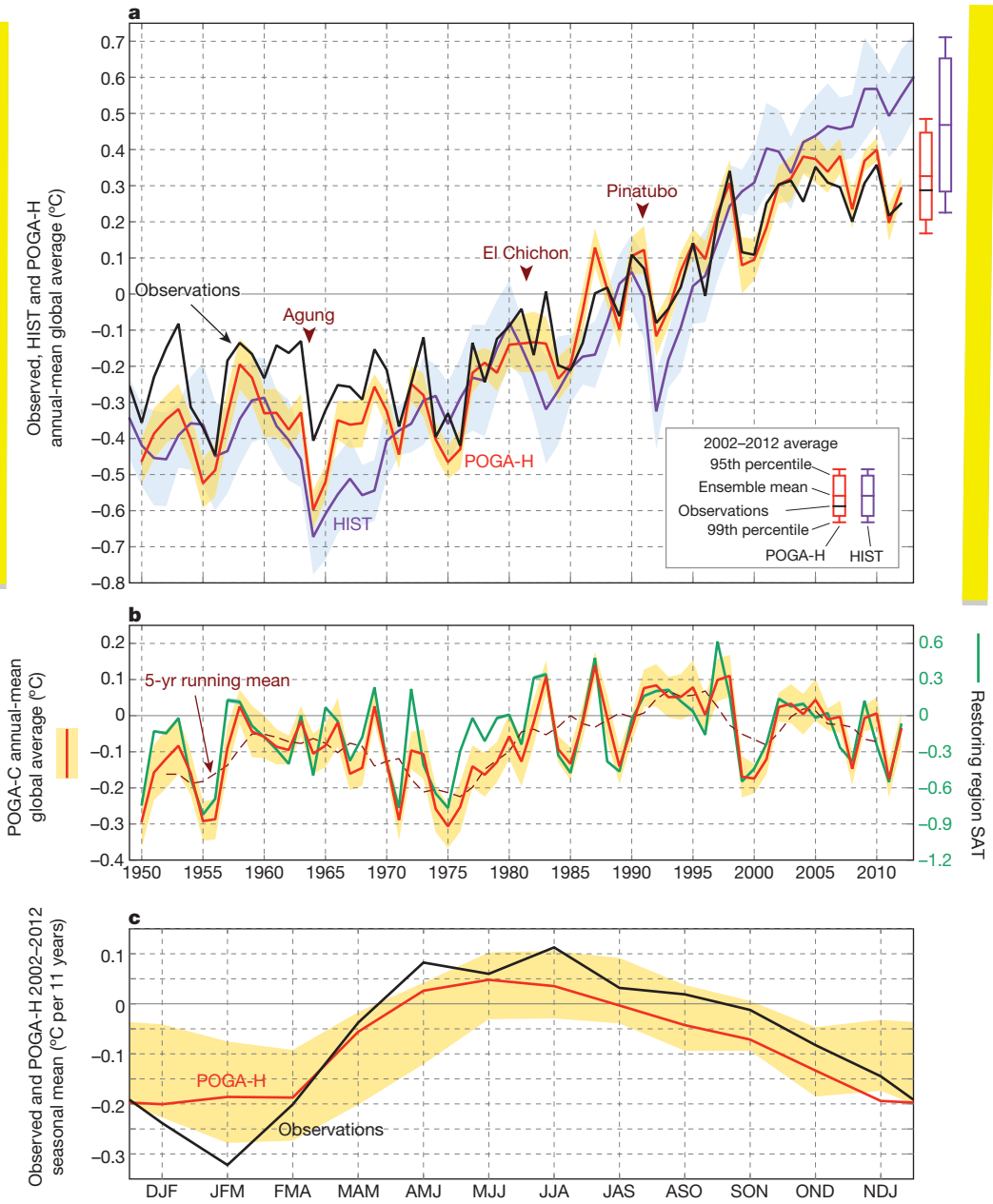

Figure 1 | Observed and simulated global temperature trends. Annual-mean time series based on observations, HIST and POGA-H (**a**) and on POGA-C (**b**). Anomalies are deviations from the 1980–1999 averages, except for HIST, for which the reference is the 1980–1999 average of POGA-H. SAT anomalies over the restoring region are plotted in **b**, with the axis on the right. Major volcanic eruptions are indicated in **a**. **c**, Trends of seasonal global temperature for 2002–2012 in observations and POGA-H. Shading represents 95% confidence interval of ensemble means. Bars on the right of **a** show the ranges of ensemble spreads of the 2002–2012 averages.

Pacific is similar in winter and in summer (Extended Data Fig. 4a), stationary/transient eddies, which are the dominant mechanism for meridional heat transport[14], are stronger in winter than summer. As a result, the tropical cooling effect on the extratropics is most pronounced in winter (the seasonality of the temperature trend in the Southern Hemisphere extratropics is weak). The tropical influence on the Northern Hemisphere extratropics is weak during the summer, allowing the radiative forcing to continue the warming trend during the recent decade (Extended Data Fig. 4b).

This seasonal contrast is evident also in HIST. For 1970–2040, a period when the ensemble-mean global temperature shows a steady increase in HIST, the probability density function for the 11-year trend is similar in winter and in summer for tropical temperatures, with means both around 0.25 °C (Extended Data Fig. 4c). The probability density function is much broader for winter than for summer for Northern Hemisphere extratropical temperatures (Extended Data Fig. 4d). The chance of the 11-year temperature change falling below –0.3 °C is 8% for winter but only 0.7% for summer in the Northern Hemisphere extratropics (around 4% in the tropics for both seasons). The 11-fold increase in the chance of an extratropical cooling in winter is partly because the tropical influence is stronger in winter than in summer.

We examined regional climate change associated with the hiatus. Although models project a slowdown of the Walker circulation in global warming[15], the Pacific Walker cell intensified during the past decade (Fig. 2c). POGA-H captures this circulation change, forced by the SST cooling across the tropical Pacific (Fig. 2d). As in interannual ENSO, the tropical Pacific cooling excites global teleconnections in December, January and February (DJF; the season is denoted by the first letters of the months). SST changes in POGA-H are in broad agreement with observations over the Indian, South Atlantic and Pacific oceans outside the restoring domain (Fig. 2a, b). The model reproduces the weakening of the Aleutian low as the response of the Pacific–North American pattern to tropical Pacific cooling[11] (Fig. 2c, d). As a result, the SAT change over North America is well reproduced, including a pronounced cooling in the northwest of the continent. The model fails to simulate the SAT and sea-level pressure (SLP) changes over Eurasia, suggesting that they are due to internal variability unrelated to tropical forcing (Extended Data Fig. 5a and c).

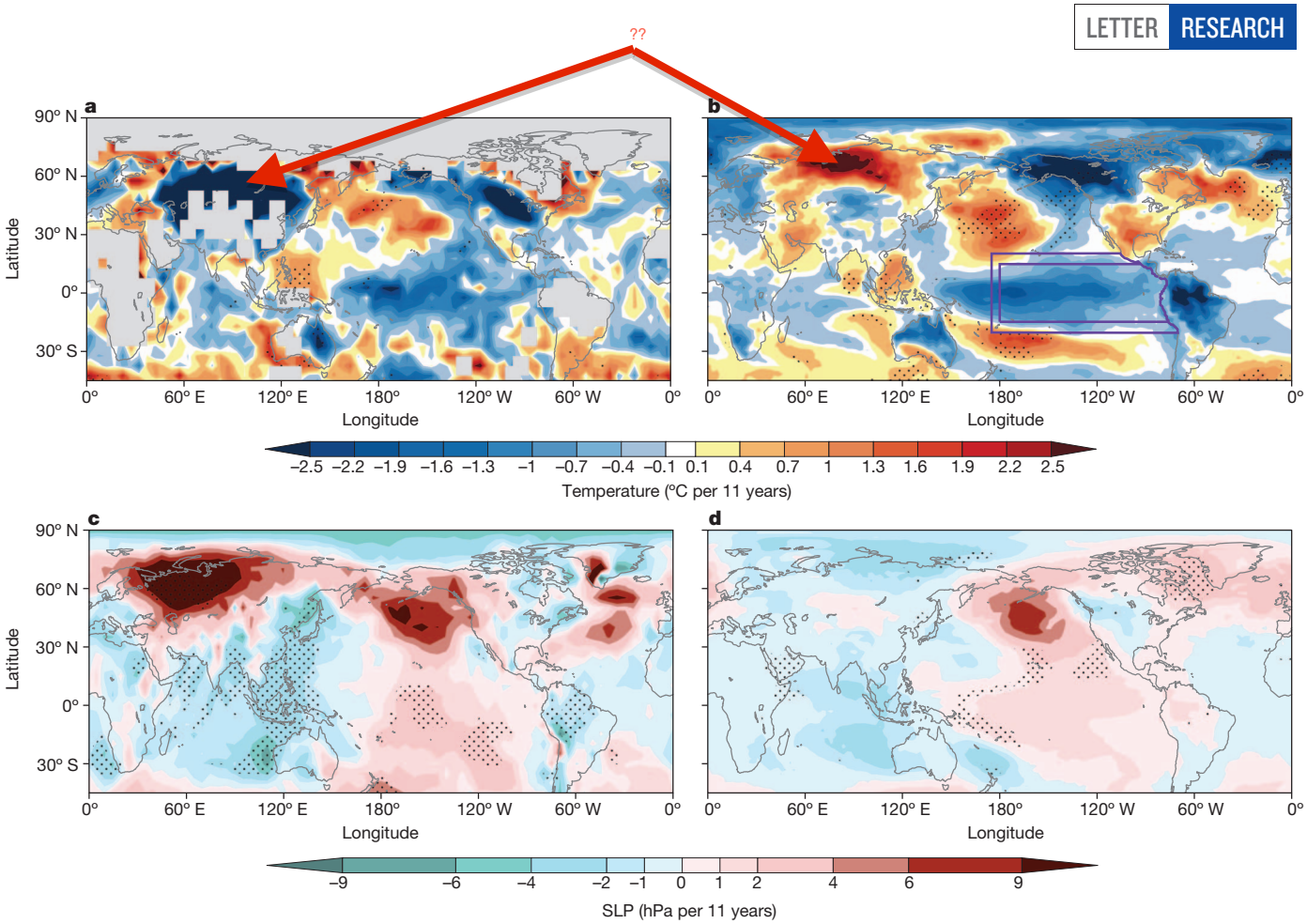

Figure 2 | Observed and simulated trend patterns in boreal winter for 2002–2012. **a** and **b** show near-surface temperature and **c** and **d** show SLP from observations (**a** and **c**) and POGA-H (**b** and **d**) in DJF. Grey shading represents missing values. Stippling indicates regions exceeding 95% statistical confidence. Purple boxes in **b** show the restoring region of POGA experiments.

In summer, the broad agreement between simulated and observed SST remains over the Pacific (Fig. 3a, b) but the tropical influence on SAT over extratropical Eurasia and Arctic is weak (Extended Data Fig. 5b), and the increasing radiative forcing permits heatwaves to develop in Northern Hemisphere continents and Arctic sea ice to melt. (The model does not produce the record shrinkage of Arctic sea ice because of model biases and natural variability in the Arctic.) We note that the observed June, July and August (JJA) warming in western midlatitude Eurasia is much more intense than in POGA-H because heatwaves there (2003 in central Europe and 2010 in Russia) are associated with long-lasting blocking events unrelated to tropical variability[16]. POGA-H captures the rainfall decrease and warming over the southern USA, changes associated with prolonged droughts of record severity in Texas[17]. The southern USA anomalies are probably tropically forced (Extended Data Fig. 5b, d and f), for which winter–spring precipitation deficits and land-surface memory processes are probably important[17]. Likewise, during the epoch of accelerated global warming from the 1970s to the late 1990s, the southern USA appears as a warming hole[18] (local warming minimum or cooling in summer), a spatial pattern that is probably tied to tropical SST (Extended Data Fig. 6).

We present here a dynamic method for quantitative attributions of decadal modulations of global warming. By prescribing observed SST over only 8.2% of the Earth's surface, POGA-H reproduces the observed time series of global-mean temperature strikingly well, including interannual to decadal variability. The comparison between HIST and POGA-H indicates that the decadal cooling of the tropical Pacific is the cause of the current hiatus. In addition, POGA-H reproduces the seasonal and key regional patterns of the hiatus. The La-Niña-like cooling in the tropics affects the extratropics strongly in boreal winter, causing global cooling, a weakened Aleutian low, and an enhanced cooling over northwestern North America among other regional anomalies. In boreal summer, in contrast, the Northern Hemisphere extratropics is largely shielded from the influence of the tropics, and the temperature continues to rise in response to the increased radiative forcing.

Whether the La-Niña-like decadal trend is internal or forced is still unclear. We note the following: (1) the tropical Pacific features pronounced low-frequency SST variability (Extended Data Fig. 7), so large that the pattern of modest forced response has not yet emerged from observations (Fig. 1b); and (2) all the climate models project a tropical Pacific warming in response to increased greenhouse gas concentrations[7]. We conclude that the recent cooling of the tropical Pacific and hence the current hiatus are probably due to natural internal variability rather than a forced response. If so, the hiatus is temporary, and global warming will return when the tropical Pacific swings back to a warm state. Similar hiatus events may occur in the future and are difficult to predict several years in advance owing to the limited predictability of tropical Pacific SST. We have shown that such events are accompanied by simultaneous characteristic regional patterns including an intensified Walker circulation, weakened Aleutian low and prolonged droughts in the southern USA.

Although the radiation-forced response will become increasingly important, deviations from the forced response are substantial at any given time, especially on regional scales[19]. We need quantitative tools—like our POGA-H—to determine the causes of regional climate anomalies[17]. The current hiatus illustrates the global influence of tropical Pacific SST, and a dependency of climate sensitivity on the spatial pattern of tropical ocean warming, which itself is uncertain in observations[20] and among models[21,22]. This highlights the need to develop predictive pattern dynamics constrained by observations.

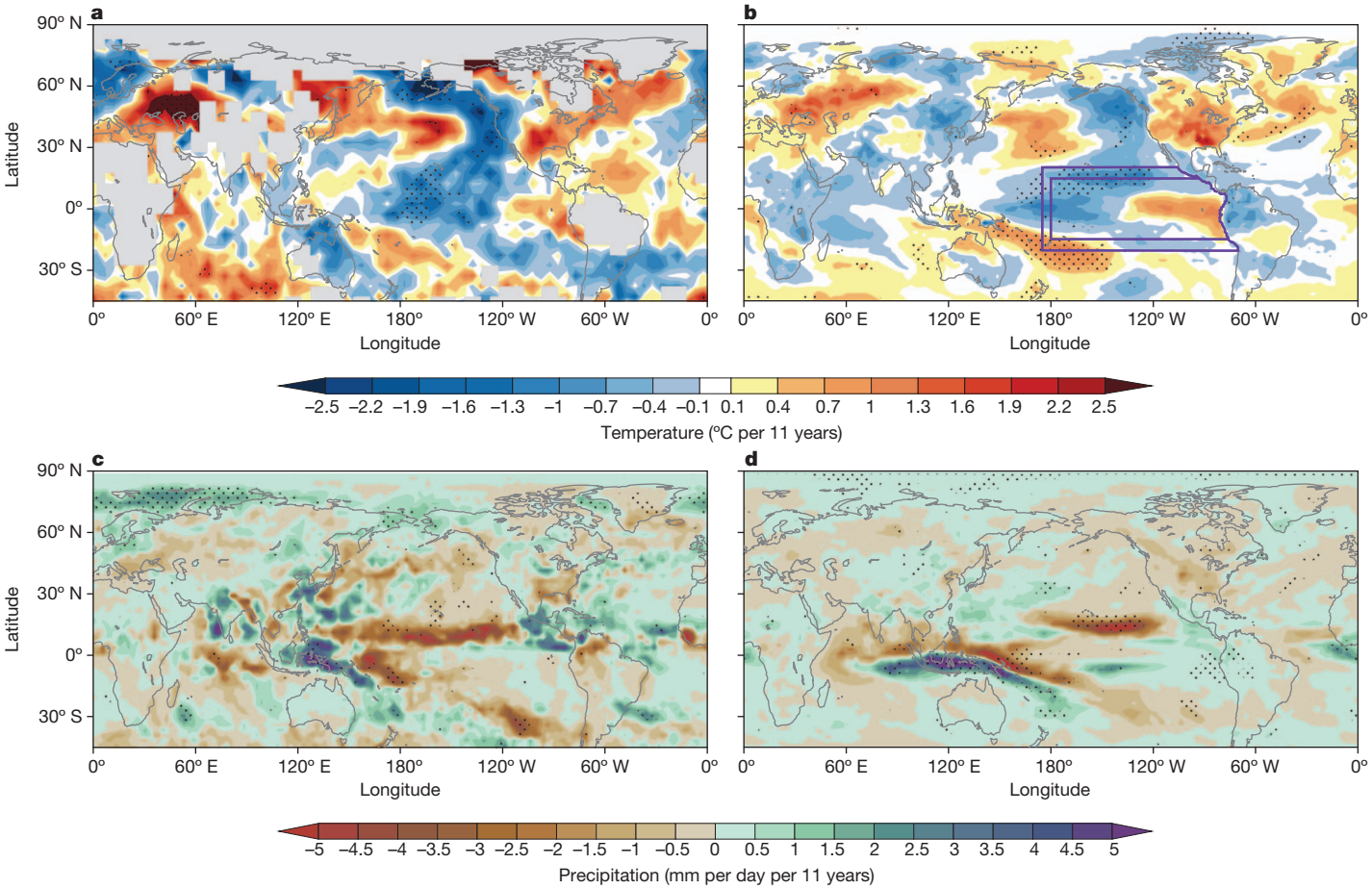

Figure 3 | Observed and simulated trend patterns in boreal summer for 2002–2012. Same as Fig. 2, except that **a** and **b** show near-surface temperature and **c** and **d** show precipitation from observations (**a** and **c**) and POGA-H (**b** and **d**) in JJA.

METHODS SUMMARY

We used the Hadley Centre–Climate Research Unit combined land SAT and SST (HadCRUT) version 4.1.1.0 (ref. 23), the Hadley Centre mean SLP data set version 2 (HadSLP2, ref. 24) and monthly precipitation data from the Global Precipitation Climatology Project (GPCP) version 2.2 (ref. 25). We examined three sets of coupled model experiments based on the Geophysical Fluid Dynamics Laboratory coupled model version 2.1 (ref. 8). HIST is forced by historical radiative forcing for 1861–2005 and Representative Concentration Pathway 4.5 (RCP4.5) for 2006–2040, based on Coupled Model Intercomparison Project phase 5 (CMIP5, ref. 26). In POGA-H and POGA-C experiments, SST is restored to the model climatology plus historical anomaly by a Newtonian cooling over the deep tropical eastern Pacific. The restoring timescale is 10 days for a 50-m-deep mixed layer. Figures 2b and 3b shows the region where SST is restored; within the inner box the ocean surface heat flux is fully overridden, while in the buffer zone between the inner and outer boxes, the flux is blended with the model-diagnosed one. In POGA-H, radiative forcing is identical to HIST, whereas it is fixed at 1990 values in POGA-C. The three experiments consist of ten member runs each.

Online Content Any additional Methods, Extended Data display items and Source Data are available in the online version of the paper; references unique to these sections appear only in the online paper.

Received 18 June; accepted 8 August 2013.
Published online 28 August 2013.

1. Easterling, D. R. & Wehner, M. F. Is the climate warming or cooling? *Geophys. Res. Lett.* **36,** L08706 (2009).
2. Foster, G. & Rahmstorf, S. Global temperature evolution 1979–2010. *Environ. Res. Lett.* **6,** 044022 (2011).
3. Solomon, S. *et al.* Contributions of stratospheric water vapor to decadal changes in the rate of global warming. *Science* **327,** 1219–1223 (2010).
4. Solomon, S. *et al.* The persistently variable "background" stratospheric aerosol layer and global climate change. *Science* **333,** 866–870 (2011).
5. Kaufmann, R. K., Kauppi, H., Mann, M. L. & Stock, J. H. Reconciling anthropogenic climate change with observed temperature 1998–2008. *Proc. Natl Acad. Sci. USA* **108,** 11790–11793 (2011).
6. Meehl, G. A., Arblaster, J. M., Fasullo, J. T., Hu, A. & Trenberth, K. E. Model-based evidence of deep-ocean heat uptake during surface-temperature hiatus periods. *Nature Clim. Change* **1,** 360–364 (2011).
7. Meehl, G. A. *et al.* in *Climate Change 2007: The Physical Science Basis* (eds Solomon, S. *et al.*). 747–845 (Cambridge University Press, 2007).
8. Delworth, T. L. *et al.* GFDL's CM2 global coupled climate models. Part I: Formulation and simulation characteristics. *J. Clim.* **19,** 643–674 (2006).
9. Zhang, Y., Wallace, J. M. & Battisti, D. S. ENSO-like interdecadal variability: 1900–93. *J. Clim.* **10,** 1004–1020 (1997).
10. Meehl, G. A., Hu, A., Arblaster, J., Fasullo, J. & Trenberth, K. E. Externally forced and internally generated decadal climate variability associated with the Interdecadal Pacific Oscillation. *J. Clim.* http://dx.doi.org/10.1175/JCLI-D-12-00548.1 (2013).
11. Alexander, M. A. *et al.* The atmospheric bridge: the influence of ENSO teleconnections on air-sea interaction over the global oceans. *J. Clim.* **15,** 2205–2231 (2002).
12. Lau, N.-C. & Nath, M. J. The role of the "atmospheric bridge" in linking tropical Pacific ENSO events to extratropical SST anomalies. *J. Clim.* **9,** 2036–2057 (1996).
13. Cohen, J. L., Furtado, J. C., Barlow, M., Alexeev, V. A. & Cherry, J. E. Asymmetric seasonal temperature trends. *Geophys. Res. Lett.* **39,** L04705 (2012).
14. Trenberth, K. E., Caron, J. M., Stepaniak, D. P. & Worley, S. Evolution of El Niño-Southern Oscillation and global atmospheric surface temperatures. *J. Geophys. Res.* **107,** AAC 5-1–17, http://dx.doi.org/10.1029/2000JD000298 (2002).
15. Vecchi, G. A. *et al.* Weakening of tropical Pacific atmospheric circulation due to anthropogenic forcing. *Nature* **441,** 73–76 (2006).
16. Barriopedro, D., García-Herrera, R., Lupo, A. R. & Hernández, E. A climatology of northern hemisphere blocking. *J. Clim.* **19,** 1042–1063 (2006).
17. Hoerling, M. *et al.* Anatomy of an extreme event. *J. Clim.* **26,** 2811–2832 (2013).
18. Wang, H. *et al.* Attribution of the seasonality and regionality in climate trends over the United States during 1950–2000. *J. Clim.* **22,** 2571–2590 (2009).
19. Deser, C., Knutti, R., Solomon, S. & Phillips, A. S. Communication of the role of natural variability in future North American climate. *Nature Clim. Change* **2,** 775–779 (2012).
20. Tokinaga, H., Xie, S.-P., Deser, C., Kosaka, Y. & Okumura, Y. M. Slowdown of the Walker circulation driven by tropical Indo-Pacific warming. *Nature* **491,** 439–443 (2012).

21. DiNezio, P. N. *et al.* Climate response of the equatorial Pacific to global warming. *J. Clim.* **22,** 4873–4892 (2009).
22. Ma, J. & Xie, S.-P. Regional patterns of sea surface temperature change: a source of uncertainty in future projections of precipitation and atmospheric circulation. *J. Clim.* **26,** 2482–2501 (2013).
23. Morice, C. P., Kennedy, J. J., Rayner, N. A. & Jones, P. D. Quantifying uncertainties in global and regional temperature change using an ensemble of observational estimates: the HadCRUT4 data set. *J. Geophys. Res.* **117,** D08101 (2012).
24. Allan, R. & Ansell, T. A new globally complete monthly historical gridded mean sea level pressure dataset (HadSLP2): 1850–2004. *J. Clim.* **19,** 5816–5842 (2006).
25. Adler, R. F. *et al.* The version-2 global precipitation climatology project (GPCP) monthly precipitation analysis (1979-present). *J. Hydrometeorol.* **4,** 1147–1167 (2003).
26. Taylor, K. E., Stouffer, R. J. & Meehl, G. A. An overview of CMIP5 and the experiment design. *Bull. Am. Meteorol. Soc.* **93,** 485–498 (2012).

Acknowledgements We thank the Geophysical Fluid Dynamics Laboratory model developers for making the coupled model version 2.1 available and L. Xu, Y. Du, N. C. Johnson and C. Deser for discussions. The work was supported by the NSF (ATM-0854365), the National Basic Research Program of China (2012CB955600), and NOAA (NA10OAR4310250).

Author Contributions Y.K. and S.-P.X. designed the model experiments. Y.K. performed the experiments and analysis. S.-P.X. and Y.K. wrote the manuscript.

Author Information Reprints and permissions information is available at www.nature.com/reprints. The authors declare no competing financial interests. Readers are welcome to comment on the online version of the paper. Correspondence and requests for materials should be addressed to S.-P.X. (sxie@ucsd.edu).

METHODS

Gridded observational data sets. We used the Hadley Centre–Climate Research Unit combined land SAT and SST (HadCRUT) version 4.1.1.0 (http://www.metoffice.gov.uk/hadobs/crutem4/; ref. 23); the Hadley Centre mean SLP data set version 2 (HadSLP2, http://www.metoffice.gov.uk/hadobs/hadslp2/; ref. 24); and monthly precipitation data from Global Precipitation Climatology Project (GPCP) version 2.2 (http://www.gewex.org/gpcp.html; ref. 25). HadCRUT is compared with the SAT of POGA and HIST.

Model experiments. We used the Geophysical Fluid Dynamics Laboratory coupled model version 2.1 (ref. 8). The HIST, POGA-H and POGA-C experiments were formed of ten member runs each. HIST is forced by the historical radiative forcing of Coupled Model Intercomparison Project phase 5 (CMIP5, ref. 26) for 1861–2005 and extends to 2040 using Representative Concentration Pathway 4.5 (RCP4.5). The forcing includes greenhouse gases, aerosols, ozone, the solar activity cycle (repeating the cycle for 1996–2008 after 2009) and land use.

In POGA experiments, the deep tropical eastern Pacific SST was restored to the model climatology plus historical anomaly by overriding the surface sensible heat flux to ocean (F) with:

$$F = (1-\alpha)F_* + \alpha(cD/\tau)(T' - T'_*)$$

Here a prime refers to the anomaly, asterisks represent model-diagnosed values, and T denotes SST. The reference temperature anomaly T' is based on Hadley Centre Ice and SST version 1 (HadISST1, http://www.metoffice.gov.uk/hadobs/hadisst/; ref. 27). The model anomaly is the deviation from the climatology of a 300-year control experiment. c is the specific heat of sea water, $D = 50$ m is the typical depth of the ocean-mixed layer, and $\tau = 10$ days is the restoring timescale. Figures 2b and 3b show the region where SST is restored: a weight $\alpha = 1$ within the inner box, linearly reduced to zero in the buffer zone from the inner to the outer boxes. In POGA-H, radiative forcing is identical to HIST, whereas it is fixed at 1990 values in POGA-C.

Trend estimates. Trends were calculated as the Sen median slope[28]. For observed surface temperature, trends were calculated for grid boxes where data are available for more than 80% of years with at least one month per season. The Mann–Kendall test was performed for the statistical significance of trends shown in Figs 2 and 3 and Extended Data Fig. 6, and Student's t-test was applied for the significance of composited differences or anomalies of trends (Extended Data Table 1 and Extended Data Fig. 2). In Extended Data Fig. 4c and d, the trends were evaluated every four years for individual members of HIST, and probability density functions were plotted with a kernel density estimation and a Gaussian smoother.

Decadal variability. In Extended Data Figs 5 and 7, the Lanczos low-pass filter with a half-power frequency of eight years was applied to extract decadal variability. Extended Data Fig. 5 shows decadal anomalies obtained from a regression analysis, with their statistical significance tested with the Student's t-statistic.

Other observational data sets. For Extended Data Fig. 1, we also used the Southern Oscillation Index (http://www.cpc.ncep.noaa.gov/data/indices/; ref. 29) and the US National Snow and Ice Data Center Arctic sea ice extent (http://nsidc.org/data/seaice_index/; ref. 30).

27. Rayner, N. A. *et al.* Global analyses of sea surface temperature, sea ice, and night marine air temperature since the late nineteenth century. *J. Geophys. Res.* **108,** 4407 (2003).
28. Sen, P. K. Estimates of the regression coefficient based on Kendall's tau. *J. Am. Stat. Assoc.* **63,** 1379–1389 (1968).
29. Trenberth, K. E. Signal versus noise in the Southern Oscillation. *Mon. Weath. Rev.* **112,** 326–332 (1984).
30. Fetterer, F. & Knowles, K. Sea ice index monitors polar ice extent. *Trans. AGU* **85,** 163 (2004).

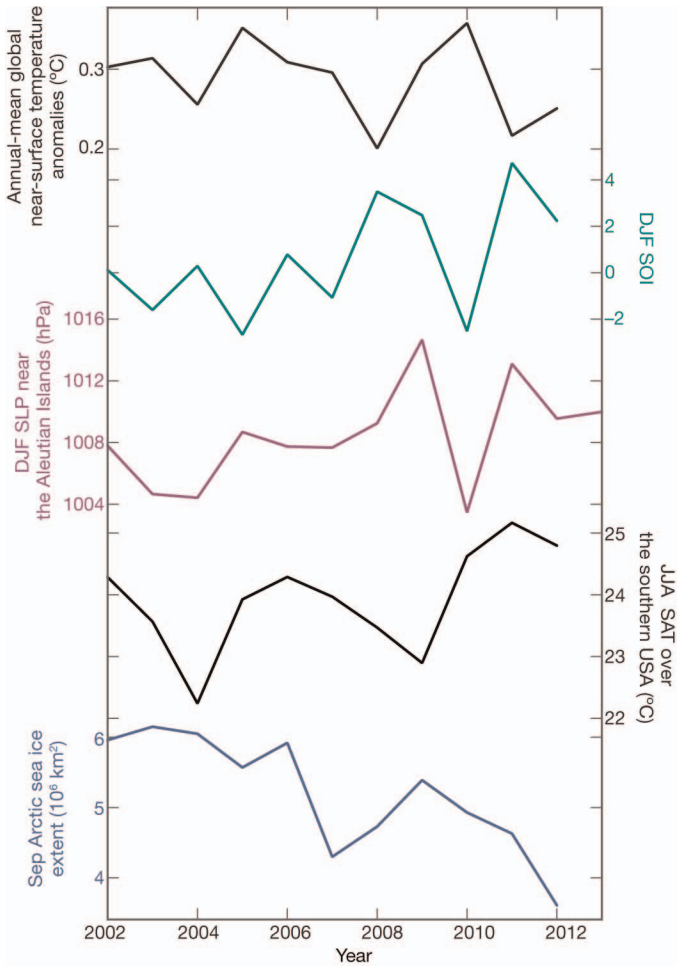

Extended Data Figure 1 | Observed climate indices for the recent decade. From top to bottom are shown the annual-mean global near-surface temperature anomalies from the 1980–1999 average, the DJF Southern Oscillation Index (SOI), the DJF SLP near the Aleutian Islands (40°–60° N, 170°–120° W), the JJA SAT over the southern USA (30°–45° N, 110°–80° W), and the September (Sep) Arctic sea ice extent.

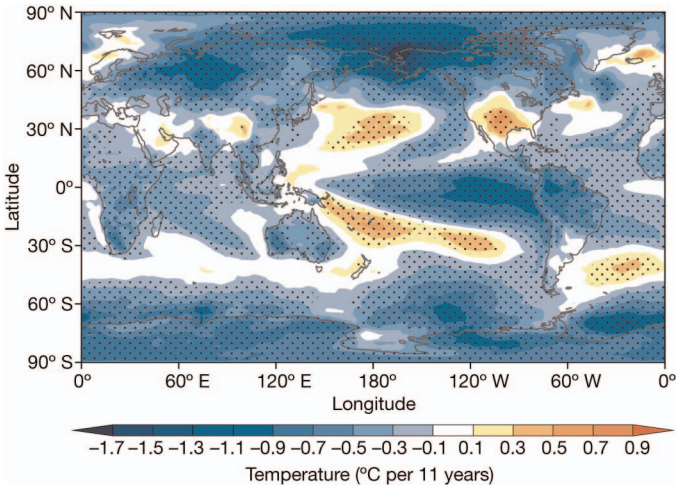

Extended Data Figure 2 | 11-year trends of annual-mean SAT composited for 34 hiatus events in HIST. The hiatus events are chosen for which annual-mean global SAT trends are smaller than their ensemble mean minus 0.3 °C per 11 years. Stippling indicates 95% statistical confidence. Note that a typical hiatus in HIST features a La-Niña-like pattern in the tropics and SST cooling around the Aleutian Islands, patterns similar to the current hiatus event.

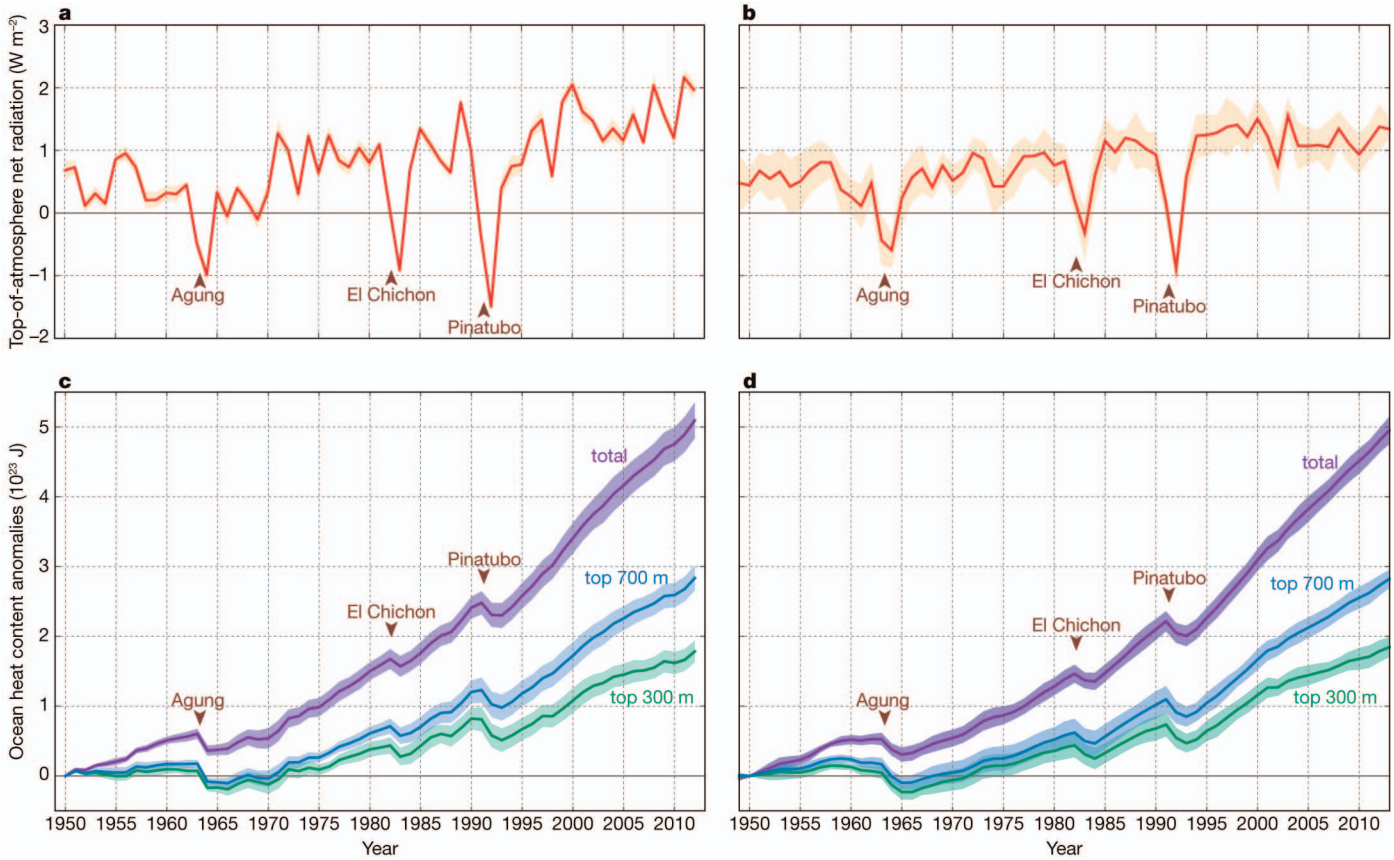

Extended Data Figure 3 | Net radiative imbalance and ocean heat content increase in POGA-H and HIST. **a**, **b**, Net radiative imbalance at the top of the atmosphere. Positive values indicate net energy flux into the planet. **c**, **d**, Ocean heat content deviations from 1950 values for each ensemble member. POGA-H (**a** and **c**) and HIST (**b** and **d**). Shading represents the 95% confidence interval of ensemble means. Major volcanic eruptions are indicated. The radiative imbalance has remained positive and ocean heat content has kept increasing for the recent decade in both of the experiments. We note that the energy budget is not closed in POGA-H.

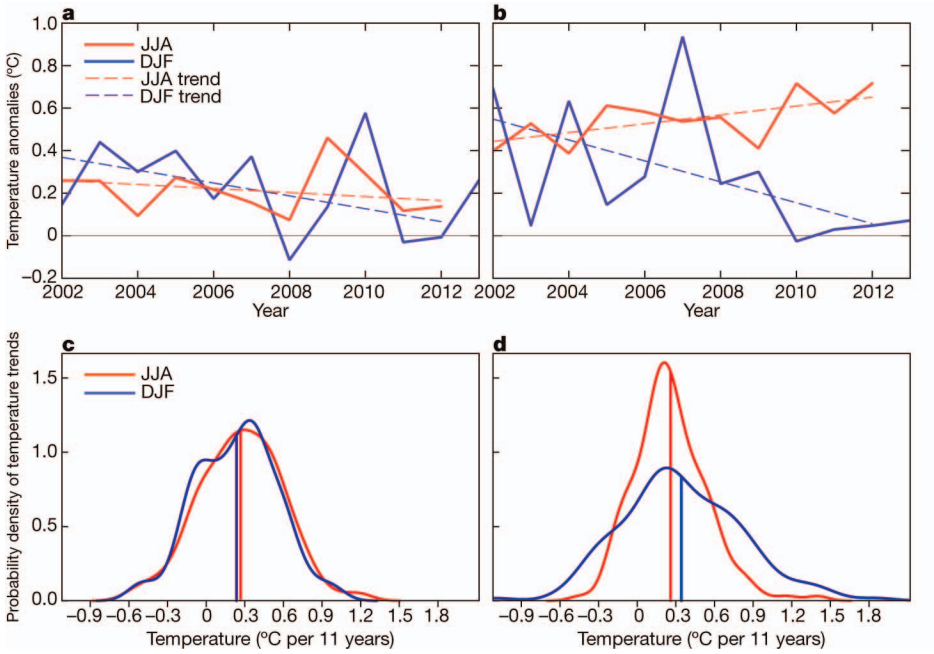

Extended Data Figure 4 | Seasonal dependency of regional temperature trends. **a**, **b**, Observed temperature anomalies (solid) and their trends (dashed) for the recent decade (°C). **c**, **d**, Probability density functions (curves) and means (vertical lines) of 11-year SAT trends in HIST for 1971–2040. Temperature has been averaged over the tropics (20° S–20° N; panels **a** and **c**) and the northern extratropics (20°–90° N; panels **b** and **d**) for JJA (red) and DJF (blue). Note that the northern extratropics features a larger probability density function spread in winter than summer, in contrast to a high similarity in the tropics. The winter spread is also greater in the extratropics than the tropics, whereas the opposite is true for summer.

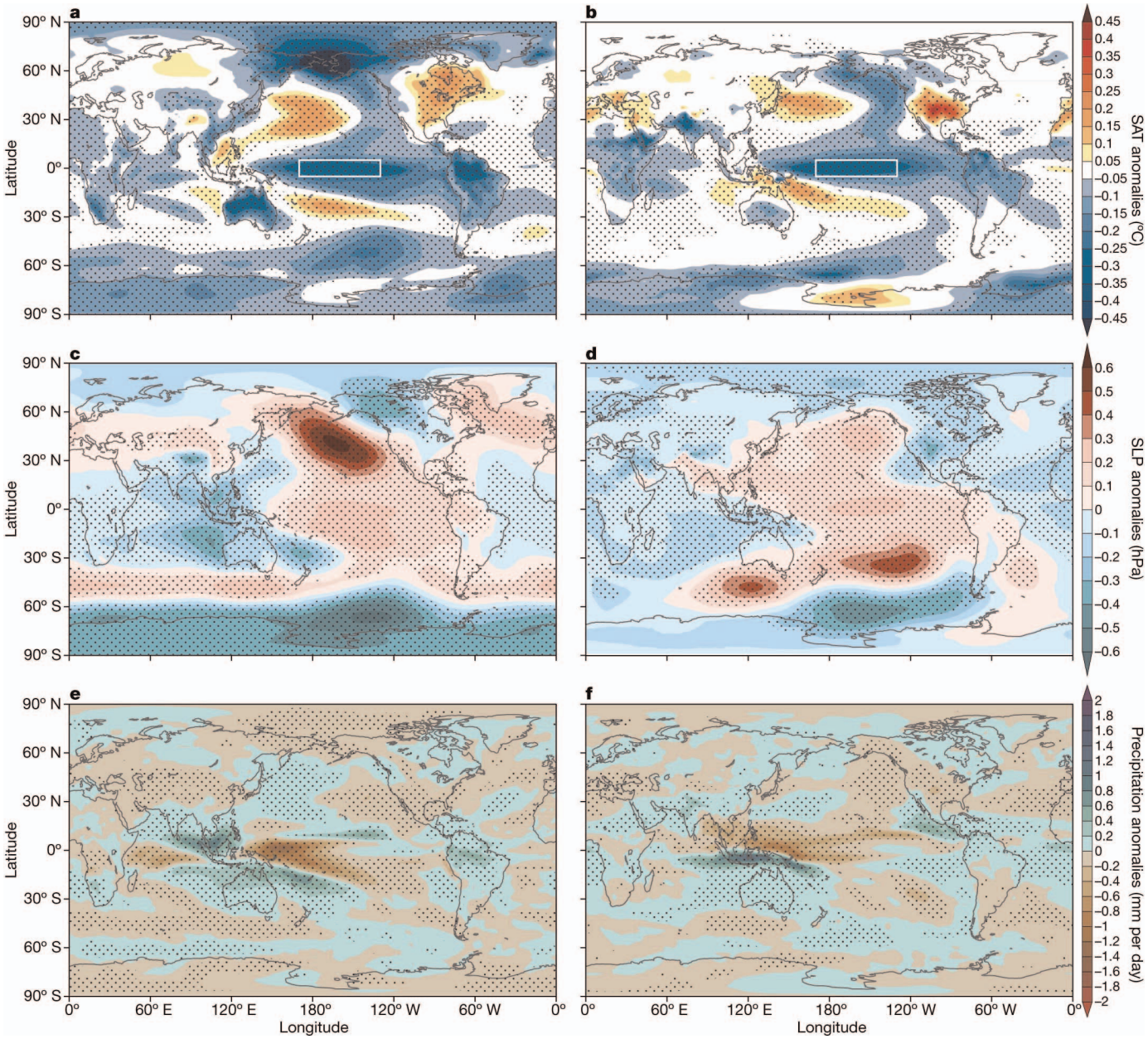

Extended Data Figure 5 | Decadal anomalies associated with SST cooling over the equatorial Pacific. Low-pass-filtered intermember anomalies in HIST regressed against SST anomalies over the area denoted by 5° S–5° N and 170° E–130° W (white boxes in **a** and **b**). **a**, **b**, SAT; **c**, **d**, SLP; **e**, **f**, Precipitation for DJF (**a**, **c**, **e**) and JJA (**b**, **d**, **f**). The sign is flipped to show a La Niña state. Stippling indicates 95% statistical confidence. We note that cold anomalies spread to the Arctic region in boreal winter but are restricted south of 60° N in summer. Anomalies in the tropics, the North Pacific and North America are broadly consistent with the trends for the current hiatus.

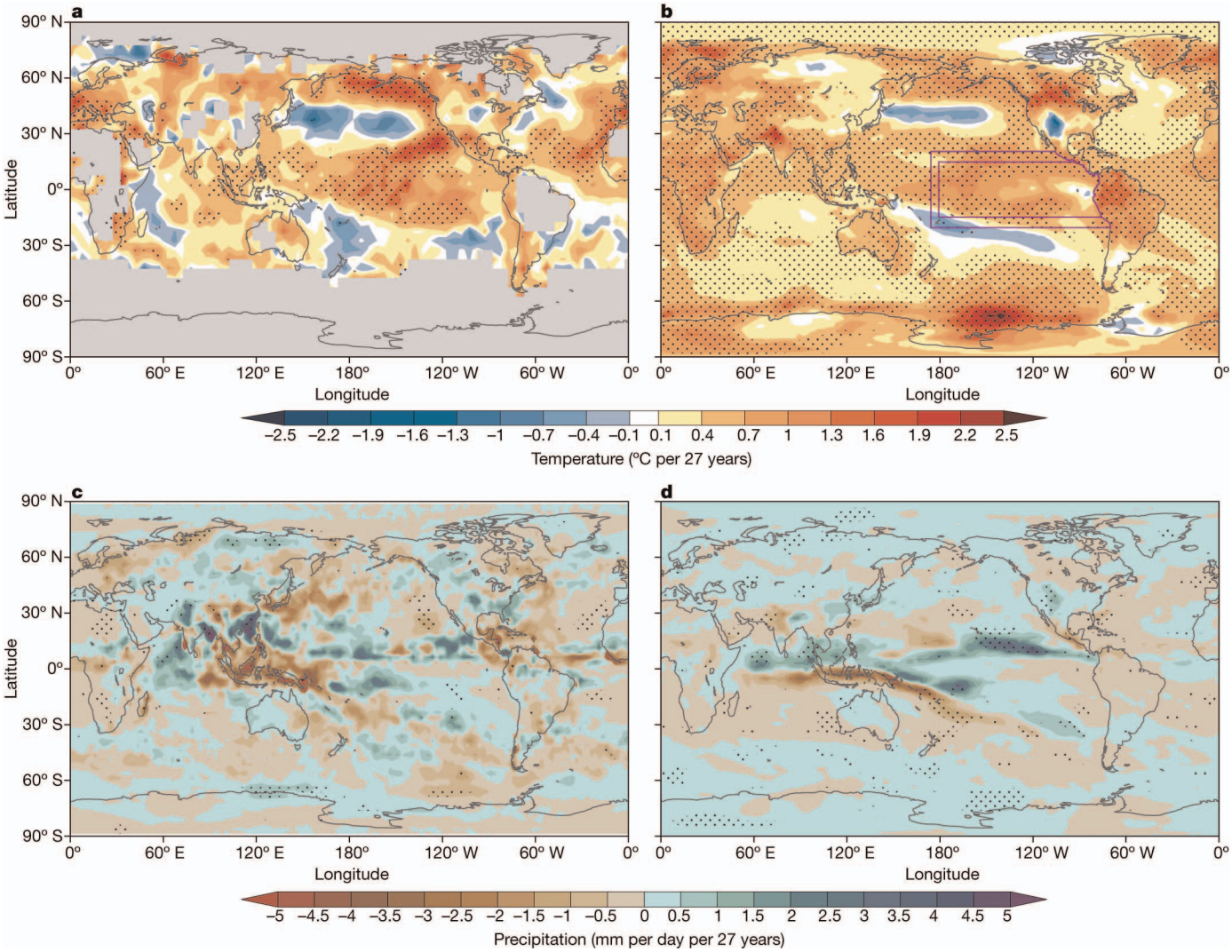

Extended Data Figure 6 | Observed and simulated trend patterns in boreal summer for the accelerated global warming period. Temperature (**a** and **b**) and precipitation (**c** and **d**) from observations (**a** and **c**) and POGA-H (**b** and **d**) in JJA. **a**, **b** and **d**, Trends for 1971–1997. **c**, The trend is evaluated for 1979–1997 and scaled to 27-year change. Stippling indicates 95% statistical confidence. Purple boxes in **b** show the restoring region of POGA experiments. We note the widespread warming, with weak cooling in the North and South Pacific oceans and a weakened Walker circulation. POGA-H reproduces the warming hole[18] (warming minimum or cooling in the central USA) with slight geographical displacements due to model biases.

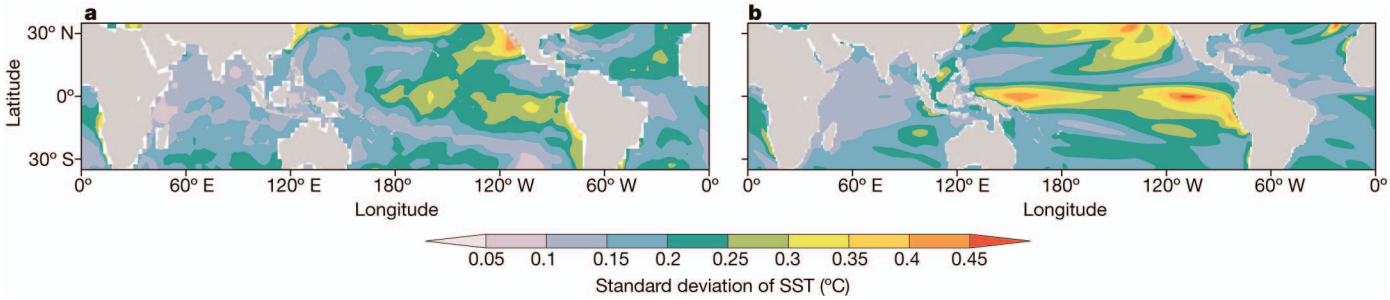

Extended Data Figure 7 | Internal decadal variability in SST. Standard deviations of annual-mean SST from observations[27] detrended for 1900-2012 (**a**) and from inter-member anomalies in HIST (**b**). Data were evaluated with a decadal low-pass filter. We note that tropical variance is most pronounced in the Pacific.

Extended Data Table 1 | Evaluation of simulations of observed global annual-mean temperature and its trend.

	Correlation coefficient		Root mean square error (°C)		Linear trends	
Experiment	Raw	Detrended	Raw	Detrended	2002-2012 (°C per 11 years)	1971-1997 (°C per 27 years)
POGA-H	0.97	0.70	0.068	0.091	–0.01	0.55
HIST	0.90	0.26	0.149	0.143	0.19	0.41

All data are based on ensemble-mean values. Correlations and root-mean-square errors are evaluated for 1970–2012 with respect to observations. The trends are significantly different between the experiments at $P < 0.01$ (2002–2012) and $P < 0.05$ (1971–1997) on the basis of Student's *t*-test applied for the ensembles.